Applied Clay Science 199 (2020) 105867

Contents lists available at ScienceDirect

Applied Clay Science

journal homepage: www.elsevier.com/locate/clay

Research Paper

Fabrication of layered double hydroxide/carbon nanomaterial for heavy metals removal

Minwang Laipan[a,b], Jianxi Zhu[a,b], Yin Xu[c,**], Luyi Sun[d,e], Runliang Zhu[a,b,*]

[a] CAS Key Laboratory of Mineralogy and Metallogeny/Guangdong Provincial Key Laboratory of Mineral Physics and Materials, Guangzhou Institute of Geochemistry, Chinese Academy of Sciences, Guangzhou 510640, China
[b] Institutions of Earth Science, Chinese Academy of Sciences, Beijing 100049, China
[c] Department of Environmental Science and Engineering, College of Environment and Resource, Xiangtan University, Xiangtan, Hunan, China
[d] Polymer Program, Institute of Materials Science, University of Connecticut, Storrs, CT 06269, USA
[e] Department of Chemical and Biomolecular Engineering, University of Connecticut, Storrs, CT 06269, USA

ARTICLE INFO

Keywords:
Layered material
Layered double hydroxide
Carbon nanosheets
Heavy metal removal

ABSTRACT

Layered double hydroxide (LDH)/sheet-shaped carbon composites are recently drawing increasing interests in various fields. Different from the conventional synthesis procedure, the composites in this work were directly prepared by in situ formation of carbon nanosheets via hydrothermal or high-temperature carbonization of organic LDH. The layered structure of LDH can be well retained after the preparation procedures and the carbon materials have sheet-like morphology evenly distributing along with LDH. The composites possess ample functional groups containing C, N, and S. Importantly, the types and relative amounts of the functional groups can be regulated via the two different carbonization methods. Abundant carboxyl and sulfonic groups are presented on the sample from hydrothermal method, while the high-temperature carbonized product mainly contains hydroxyl and thiophenol/thiol. These two different carbonization strategies also cause large differences in specific surface area of the composites; high-temperature carbonization treatment favors the production of large specific surface area. LDH/carbon nanosheets show much better adsorption performance than LDH toward both Cr(VI) and Cd(II), with maximum of 4.4- and 6.7-fold increase of the adsorbed capacities, respectively. This work provides facile ways for preparation of LDH/carbon nanosheets materials, which may also be ways for recycling of waste organic clay and organic clay minerals by producing functional materials.

1. Introduction

Two-dimensional (2D) nanomaterials are currently a topic of significant interest due to their extraordinary physiochemical properties. They are potentially useful in a wide range of applications such as environmental remediation, catalytic degradation/synthesis, and energy storage (Koilraj et al., 2018b; Ma et al., 2016; Ma et al., 2015; Wan et al., 2016). Layered double hydroxides (LDH), previously known as anionic clays, are one type of 2D materials that have attracted significant interests in recent years (Aregay et al., 2019; Jawad et al., 2019; Laipan et al., 2020b). LDH comprise of positively charged metal hydroxide layers sandwiched by charge compensating interlayer anions with optional solvation e.g. water (Yu et al., 2017a). LDH have become the focus for both fundamental researches and practical applications due to their unique structures, tunable chemical compositions, and a wide variety of material properties (Jawad et al., 2018; Li et al., 2014; Wang and O'Hare, 2012; Xu et al., 2018; Yao et al., 2019).

Despite the unique intrinsic properties of LDH, various functionalization strategies have been applied to LDH that yield even more exciting performance opportunities (Jawad et al., 2017; Koilraj et al., 2018a; Laipan et al., 2020a; Laipan et al., 2020b; Li et al., 2014; Wan et al., 2016). Recently, loading sheet-shaped carbon materials such as graphene, graphite oxide, and other carbon nanosheets onto LDH surface to form 2D LDH/sheet-shaped carbon nano composites has been recognized as an effective functionalization strategy, and the resultant materials have been widely investigated for environmental and energy related applications (Cao et al., 2016; Daud et al., 2016; Pang et al., 2019). These hybrids combine the properties arising from both carbon and LDH (Cao et al., 2016; Daud et al., 2016; Pang et al., 2019; Zhao et al., 2014). Carbon provides large exposed surfaces and specific facets, which can offer ample functional groups and high active surface sites that can effectively promote the activity of the composite (e.g.,

* Correspondence to: Runliang Zhu, Guangzhou Institute of Geochemistry, Chinese Academy of Sciences, Guangzhou 510640, China.
** Corresponding author.
E-mail addresses: xuyin@xtu.edu.cn (Y. Xu), zhurl@gig.ac.cn (R. Zhu).

https://doi.org/10.1016/j.clay.2020.105867
Received 11 May 2020; Received in revised form 18 September 2020; Accepted 25 September 2020
Available online 08 October 2020
0169-1317/

adsorptive and electric performance) (Hou et al., 2017), whilst LDH can effectively reduce the aggregation of carbon nanomaterial and retain the abilities of LDH such as adsorptive and catalytic performance (Pang et al., 2019). These hybrid nanomaterials are expected to be of great application prospect in environmental and energy fields (Cao et al., 2016; Daud et al., 2016; Le et al., 2019; Pang et al., 2019). For example, Gunjakar et al. (2013) assembled a highly effective photocatalyst by combining ZnCr-LDH with graphene nanosheets. The resultant material gave a remarkable depression of the photoluminescence signal, and an unusually high photocatalytic activity for visible light-induced O_2 generation with a rate twice higher than that of the pristine ZnCr-LDH. Yu et al. (2017b) applied nanocomposite of graphene oxide and NiAl-LDH to capture radionuclide of U^{VI} and found that the maximum removal capacity on the composite was 2.3-fold higher than that of the pure NiAl-LDH. Similar results can also be found by using composite of graphene oxide and MgAl-LDH as U^{VI} adsorbent (Linghu et al., 2017). Nonetheless, facilely producing high quality and large quantity of 2D nanomaterials is still a concerned challenge (Hou et al., 2017).

LDH/sheet-shaped carbon nanomaterials are conventionally prepared by employing pre-synthesized sheet-shaped carbon as raw material to in-situ grow LDH via hydrothermal, coprecipitation, solvothermal, microwave, or electrochemical methods, or using both pre-prepared sheet-shaped carbon C and LDH to fabricate the composites by exfoliation-restacking and layer-by-layer pathways (Cao et al., 2016; Daud et al., 2016; Le et al., 2019; Li et al., 2010; Pang et al., 2019). To the best of our knowledge, no study however, has been directed to the preparation of the composites by in situ forming carbon nanosheet during the preparation process. Several previous studies indicated that layered materials could be well templates for preparing sheet-shaped carbon. For example, graphene nanosheets or graphene-like carbon nanosheets can be synthesized via carbonizing the intercalated organic matters in the confined interlayer space of the 2D galleries of montmorillonite or LDH (Chen et al., 2014; Chen et al., 2019; Laipan et al., 2015; Sun et al., 2012). Our previous studies suggested that LDH layers could be well template for growing carbon nanosheets (Laipan et al., 2015). LDH possess “memory effect” which means that their calcined products can rehydrate and recover to LDH in aqueous environment (Miyata, 1980; Peng et al., 2016; Zhao et al., 2012), and therefore fabricating LDH/carbon nanosheets may be readily achieved via high-temperature carbonization of organic LDH and follows by reacting with water. As shown in a number of studies, the functional groups of carbon were critical in improving activities of LDH/carbon composite (Cao et al., 2016; Daud et al., 2016). Our previous studies indicated that carbon nanosheets prepared by using LDH as template possessed ample functional groups, but the type and relative contents of the functional groups were difficult to regulate via high-temperature carbonization method (Laipan et al., 2015). On the other hand, the newly developed hydrothermal carbonization procedure is also a powerful method to synthesize carbon materials with characteristic of ample and controllable functional groups (Latham et al., 2018; Wen et al., 2017). As the hydrothermal carbonization procedure is generally conducted at relatively low temperature (150–350 °C) (Nizamuddin et al., 2017), it may also be a powerful in-situ way to prepare LDH/sheet-shaped carbon which will probably retain LDH structures during hydrothermal carbonization of organic LDH. Through these different strategies, we may conveniently adjust the carbon nanosheets with different surface structures, and consequently obtain LDH/carbon nanosheets composites with different structure and properties.

Herein, we report simple synthesis methods for LDH/sheet-shaped carbon by transformation of organic compounds into sheet-shaped carbon on organic LDH. As LDH are commercially available (and spent LDH adsorbents generated from adsorption of organic contaminants can also be the precursors), large-scale synthesis of 2D LDH/carbon nanosheets becomes possible. As proposed above, the prepared LDH/carbon nanosheets composites may have flaky morphology and ample functional groups, and therefore they may have various potential applications (e.g. contaminants removal). This study firstly attempted to compare the differences in properties of the nanomaterials produced from the two different carbonization methods, and then examined the performance of the resultant materials by removal of heavy metal ions. It is expected to provide simple ways for recycling of waste organic clay and organic clay minerals by producing functional materials via this study.

2. Experimental details

2.1. Materials

$Cd(NO_3)_2{\cdot}4H_2O$ (99.0%), $K_2Cr_2O_7$ (99.0%), and organic dye orange II (OII, $C_{16}H_{11}N_2SO_4Na$) were purchased from Aladdin-E. NaOH and HNO_3 were purchased from Guangzhou chemical reagent CO., LTD (Guangzhou, China). All chemicals were used as received. MgAl-LDH (99.0%, molar ration of Mg/Al = 2) with CO_3^{2-} located in the interlayers was purchased from Hunan Shaoyang Tiantang Auxiliaries Chemical CO., LTD (Hunan, China). Its structural data (XRD, BET, and SEM image) can be seen in our previous research (Laipan et al., 2018).

2.2. Preparation of LDH-OII hybrids

Organic LDH was prepared by reconstructing LDH structure in OII solution by using memory effect of LDH. MgAl-LDH was first calcined at 500 °C for 3 h to obtain calcined LDH (CLDH) (Laipan et al., 2015), following which CLDH was then disperse in OII solution in a bottle with cover. In detail, 5 g of CLDH were added into 1 L of 0.02 M OII solution, resulting in LDH-OII hybrids with OII adsorbed amounts of 1390.4 mg (OII)/g (CLDH). The hybrids are denoted as LDH-OII.

2.3. Preparation of LDH/carbon nanosheets composites

2.3.1. High-temperature carbonization plus reconstruction method

Pyrolysis of LDH-OII hybrid was performed in a tubular furnace under constant nitrogen flow according to the previous method (Laipan et al., 2017b; Laipan et al., 2016). In detail, the dried LDH-OII powders were loaded to a crucible, and then heated in a temperature-controlled tubular furnace to the required temperature. The heating rate was 10 °C/min, and the samples were maintained at 600 °C for 3 h. The carbonization temperatures were chosen according to the results of TG analysis in our previous work (Laipan et al., 2015). The resultant composites were soaked in deionized water (in a bottle with a lid to prevent the absorption of CO_2 from air) for 12 h to restore the LDH structures. The final composite produced from LDH-OII is denoted as LDH-carbon.

2.3.2. Hydrothermal carbonization method

LDH-OII was selected to perform hydrothermal carbonization experiment. In a typical procedure, 5 g of LDH-OII were first dispersed in 20 mL deionized water. The suspension was then transferred to a 50 mL polytetrafluoroethylene-lined autoclave and heated at 250 °C for 24 h. According to previous reports, hydrothermal carbon (HTC) could be produced at temperature range of 150–350 °C, (Jain et al., 2016) therefore we selected a moderate temperature of 250 °C. The resultant material hereafter is named as LDH-HTC. On the other hand, the control sample of reconstructed LDH (R-LDH) in water rather than in OII solution was also hydrothermal treated, and the resultant sample is called as LDH-HT. Finally, carbon materials were also produced by acid washing of LDH-HTC and LDH-carbon to conduct proper analysis. The carbon materials resultant from LDH-HTC and LDH-carbon are named as HTC and Carbon, respectively.

For clarity, a scheme (Scheme 1) was made to illustrate the preparation diagram and the construction of composites.

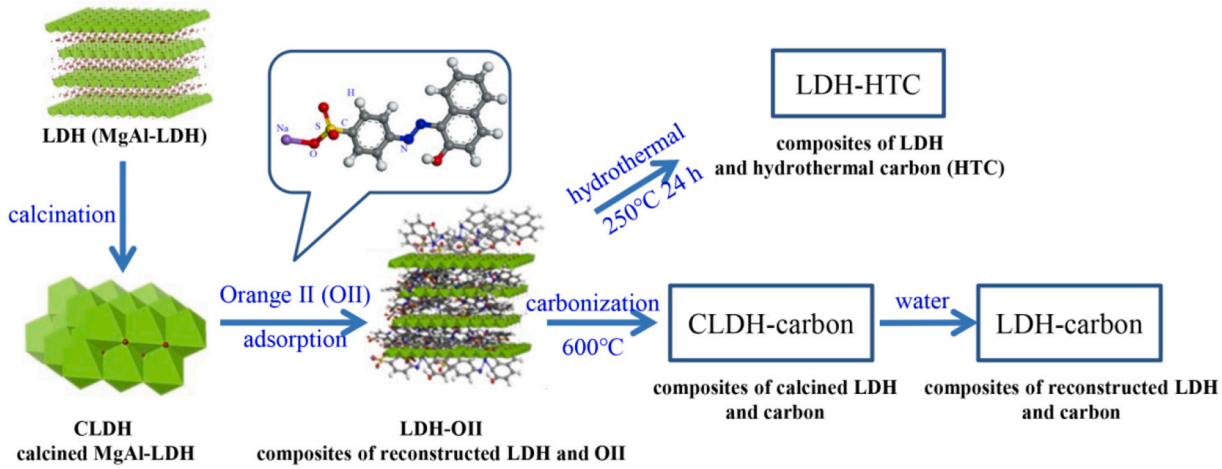

Scheme 1. Preparation procedures and nomenclature of the materials.

2.4. Characterization methods

X-ray diffraction (XRD) patterns of the samples were measured on a Bruker D8 ADVANCE X-ray diffractometer using Cu Kα radiation operating at 40 kV and 40 mA. The patterns were recorded over the 2θ range from 3° to 70° with a scan speed of 3°/min using a bracket sample holder. X-ray photoelectron spectroscopy (XPS) spectra were recorded using a Kα X-ray photoelectron spectrometer (Thermo Fisher Scientific, UK) with a monochromatic Al Kα X-ray source. All spectra were calibrated using a C 1 s peak with a fixed value of 284.8 eV. After calibration, the background from each spectrum was subtracted using a Smart-type background to remove most of the extrinsic loss structure. Transmission electron microscopy (TEM) images were acquired using FEI Talos F200S high resolution TEM instrument at an acceleration voltage of 200 kV. The instrument is equipped with HAADF detector and energy dispersive X-ray spectroscopy (EDS) for the determination of composition and elemental distribution of the samples. Atomic force microscope (AFM) analysis was carried out on a Bruker Nanoscope IVa scanning probe microscope (Digital Instruments, Santa Barbara, CA) at room temperature (25 °C). Infrared spectra of the samples were obtained by using a Bruker Vertex–70 FTIR spectrophotometer via KBr pressed-disk technique. Specific surface area was determined at 77 K using an ASAP 2020 Surface Area & Pore Size Analyzer (Micromeritics Instrument Corporation). Specific surface area was calculated using the Brunauer-Emmett-Teller (BET) method. The zeta potentials of all the samples were determined by Mastersizer NANO ZS (Malvern Instrument Limited, England).

2.5. Cd(II) and Cr(VI) adsorption experiments

2.5.1. Cd(II) adsorption

1 L Cd(II) solution with concentration of 10 mmol/L (pH 5.0) was prepared using nitrate. Batch adsorption experiments were carried out using glass tubes with covers (to avoid the influence of CO_2 from atmosphere) at 25 °C on a shaker with a shaking speed of 200 rpm for 12 h. Experimental solution pH was adjusted to 7.0 after adding LDH, and the concentrations of Cd(II) varied from 0.2 to 1.5 mmol/L (22.4–168.0 mg/L). In every experiment, about 50 mg of each composite was dispersed in 50 mL of Cd(II) solution with varying concentrations. After 12 h, the supernatant was collected by centrifugation and then analyzed by atomic absorbance spectrometer (PE AAnalyst 400) to determine the concentrations of the remnants Cd(II). All of the experiments were conducted twice.

2.5.2. Cr(VI) adsorption

Cr(VI) removal experiments were conducted using glass vials in a batch equilibrium technique in aqueous solution at pH 7.0 and room temperature. The dosage of the composite was 1 g/L and Cr(VI) concentrations varied from 5 to 100 mg/L, with the contact time being 12 h. At the given contact time, the reaction solution was sampled and filtered through 0.22 μm membrane. Concentrations of Cr(VI) were quantified at 540 nm, using 1, 5-diphenylcarbazide in acid solution as the complexing agent (Laipan et al., 2017a; Laipan et al., 2017b; Liu et al., 2019). All of the experiments were conducted twice.

2.6. Regeneration of the adsorbents

For the renewal of sorbents, an adsorption – desorption procedure was used. Taking the regeneration of adsorbents after adsorption of Cr(VI) as an example, the composites were first used to adsorb Cr (VI). After that, 1 mol/L NaCl solution was applied to desorb Cr(VI) from the composites to achieve the regeneration of the adsorbents. The renewed adsorbents were employed to adsorb Cr(VI) again. The adsorption – desorption cycles were performed 5 times. The regeneration of adsorbents after adsorption of Cd(II) also used the adsorption – desorption procedure, with the only difference of replacing of NaCl by CH_3COONa. According to the previous studies, Cd (II) could be well desorbed by using CH_3COONa (Mallakpour and Behranvand, 2017).

3. Results and discussion

3.1. Structure and morphology of the composites

The crystal structure and phase identification of the materials were revealed by XRD analysis as shown in Fig. 1. The XRD pattern of the reconstructed LDH (R-LDH) from CLDH via reaction with water in open air atmosphere indicates that R-LDH was well crystallized with the only characteristic reflections belonging to MgAl-LDH (PDF#89–0460). The adsorption of OII resulted in the distribution of OII in the interlayers and on the outer surface of LDH indicated by the XRD patterns of LDH-OII and OII. As shown in XRD pattern of LDH-OII, reflection at c.a. 3.7° (d value of 2.30–2.42 nm) may belongs to the combination reflection of the OII and expansive (003) of LDH by intercalation of OII as suggested by the diffraction peak at c.a. 7.4° (d value of 1.14–1.19 nm) which should be the secondary diffraction peak of (003) (i.e., (006)). As d value of 2.30–2.42 nm is larger than twice the d value of 1.14–1.19 nm, we deduce the reflection at c.a. 3.7° belongs to the combination reflection of the OII and expansive (003). The distribution characteristics of OII suggest that in the carbonized products probably presents LDH-carbon-LDH alternating interval layered structures if the obtained carbon materials possess a flake-like morphology. After hydrothermal

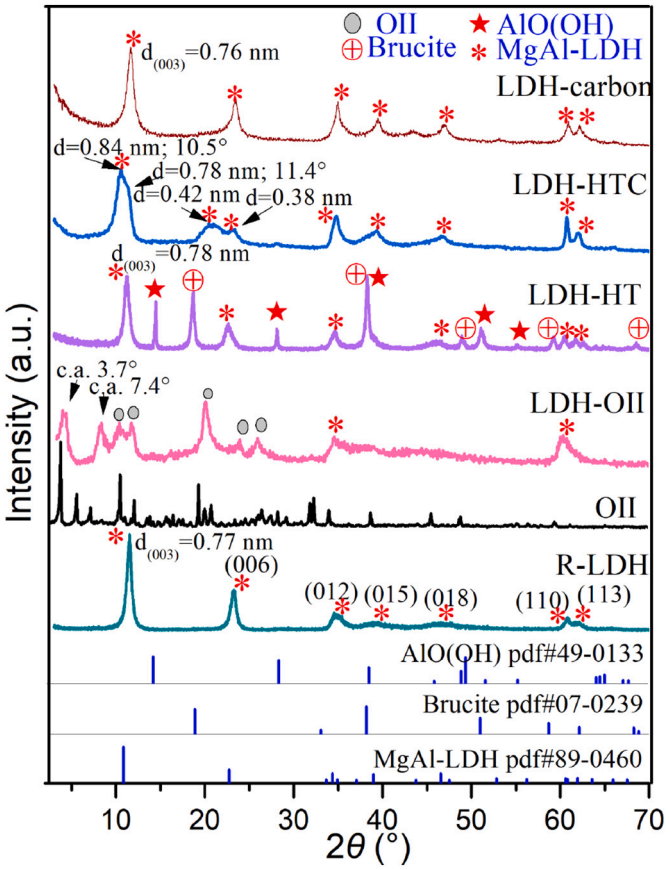

Fig. 1. XRD patterns of the composites of LDH and carbon materials (LDH-carbon and LDH-HTC) and their precursors. R-LDH in the figure represents the reconstructed LDH from CLDH via reaction with water in open air atmosphere (i.e., the interlayer anions should be carbonate); the composites have LDH structure.

carbonization of LDH-OII, the resultant LDH-HTC shows only the characteristic reflections belonging to MgAl-LDH, indicating the retention of LDH structures. However, it should be noted that the reflection at 2θ of 9.0–12.3° should be the combination of two peaks as suggested by the asymmetry shape. One with d value of 0.84 nm belongs to the expansive (003) of LDH, and the other with d value of 0.78 nm attributes to the pristine (003) of the LDH. The existence of secondary diffraction peaks in the range of 20–25° of expansive and pristine (003) respectively with d values of 0.42 and 0.38 nm is the evidence. The basal spacing of 0.84 nm for LDH-HTC is larger than those of R-LDH and LDH-HT, suggesting the existence of carbon materials in the LDH interlayers. Deduced from the distance between two LDH layers (0.84–0.48 = 0.36 nm; 0.48 nm is the theoretical thickness of an LDH single layer(Yu et al., 2015)), it is suggested that maximum of 1 layer of carbon layer (thickness of single carbon layer is 0.34 nm (Rafiee et al., 2012)) is presented in the interlayer of LDH. The comparison between XRD patterns of LDH-HTC and LDH-HT suggests that the presence of OII can protect the LDH structures and prevent the formation of impurity during hydrothermal carbonization. According to the XRD patterns of the LDH-carbon, LDH structures can be well reconstructed through conventional high-temperature carbonization plus water washing treatment. But no carbon layer may exist in the interlayer of LDH because the distance between two LDH layers is 0.76–0.48 = 0.28 nm (less than the thickness of single carbon layer). Therefore, the two different carbonization methods produced different products with differences in the arrangements of LDH and carbon nanosheets. On the other hand, the two different carbonization methods also caused differences in degrees of crystallinity of LDH. The degrees of crystallinity of LDH in the two composites were calculated by K-value method, and results show that LDH-carbon possesses more crystalline LDH (56.2%) than that of LDH-HTC (46.9%) (Fig. S1). This difference may be caused by the differences in relative distribution between LDH and carbon materials.

TEM images of the LDH/carbon composites are shown in Fig. 2, from which it can be seen that LDH-HTC, LDH-carbon, LDH-HT, and R-LDH all present sheet-like morphologies. The sheet-like morphology of LDH-HTC and LDH-carbon demonstrates the formation of LDH/carbon nanosheets composites. Additionally, AFM and TEM results of the carbon materials resultant from acid washing of LDH-HTC and LDH-carbon further demonstrate the formation of carbon nanosheets (Fig. S2). For HTC from LDH-HTC, it has lateral dimension of 30–140 nm and thickness of 0.66–2.08 nm. For Carbon from LDH-carbon, it has typical flaky morphology with micron-sized lateral dimension and thickness of 0.64–1.97 nm. The results indicate that LDH layers are reliable layered templates for flake-like morphology carbon growth during hydrothermal and conventional carbonization. Hydrothermal carbonization favors the preparation of small laterally sized carbon nanosheets, while conventional carbonization method is beneficial to produce large laterally sized carbon nanosheets. According to the elemental mapping results (Fig. 3), carbon element is evenly distributed along with Mg and Al elements in the composites of LDH/carbon nanosheets produced from both hydrothermal and conventional high-temperature carbonization procedures using a same precursor (LDH-OII). Additionally, FTIR results (Fig. 4) suggest that the carbon element is attributed to the carbon materials in the composites rather than carbonate ions, because there are no carbonate stretching modes (632 cm^{-1} for ν_4, 826 cm^{-1} for ν_2, and 1384 cm^{-1} for ν_3 (Chen and Qu, 2003)) in the LDH-HTC and LDH-carbon. These results indicate the uniform distribution of carbon nanosheets with LDH layers.

3.2. Functional groups and surface area characterization of the composites

FTIR spectra were applied to analyze the surface functional groups of the LDH/carbon nanosheets composites (Fig. 4). According to the guiding books of infrared spectroscopy (Colthup, 2012; Larkin, 2017), there are −OH, −COOH, $-SO_3$, benzene rings, and/or −C−O/−C═O/$-NO_2$/$-NH_3$ in the LDH/carbon nanosheets composites. XPS spectra were further employed to reveal the surface functional groups of the LDH/carbon nanosheets composites. XPS spectra of C 1 s, S 2p, and N 1 s of the obtained composites were plotted, and peaks were further deconvolved (Fig. 5). The elements of C, S, and N are derived from the organic dyes of OII, which were demonstrated to be sources of the ample functional groups. Different from the C 1 s spectrum of R-LDH (Fig. S3), the C 1 s spectra of LDH-HTC and LDH-carbon can be deconvoluted into four peaks, which are assigned to graphitized or amorphous carbon (284.8 eV), C−OH/C═N (285.9 eV), C═O/C−N (287.6 eV), and O═C−OH (289.2–289.7 eV), respectively. (Clearfield and Costantino, 1996; Damodar et al., 2018; Hou et al., 2017; Khan et al., 2009; Laipan et al., 2015; Terzyk, 2001; Whittingham and Jacobson, 1982; Yang et al., 2009; Zhou et al., 2007) As suggested by C 1 s spectra, hydroxyl/C═N and carboxyl are the dominant C-involved functional groups on these LDH/carbon nanosheets composites, but different carbonization treatment can adjust their relative contents. Hydrothermal carbonization led to higher amount of carboxyl than that of hydroxyl/C═N groups, while high-temperature carbonization treatment caused a higher amount of hydroxyl/C═N than that of carboxyl.

LDH-HTC and LDH-carbon show completely different S 2p spectra. Sulfonic and thiophenol/thiol groups are the major functional groups on these LDH/carbon nanosheets composites. Hydrothermal carbonization retained sulfonic group ($-SO_3$, 168.5 eV for S 2p3/2) from organic dyes OII and produced no other S-involved functional group. Via conventional high-temperature carbonization treatment however, thiophenol/thiol (PhSH/RSH) (S 2p3/2 and S 2p1/2 at 163.9 and

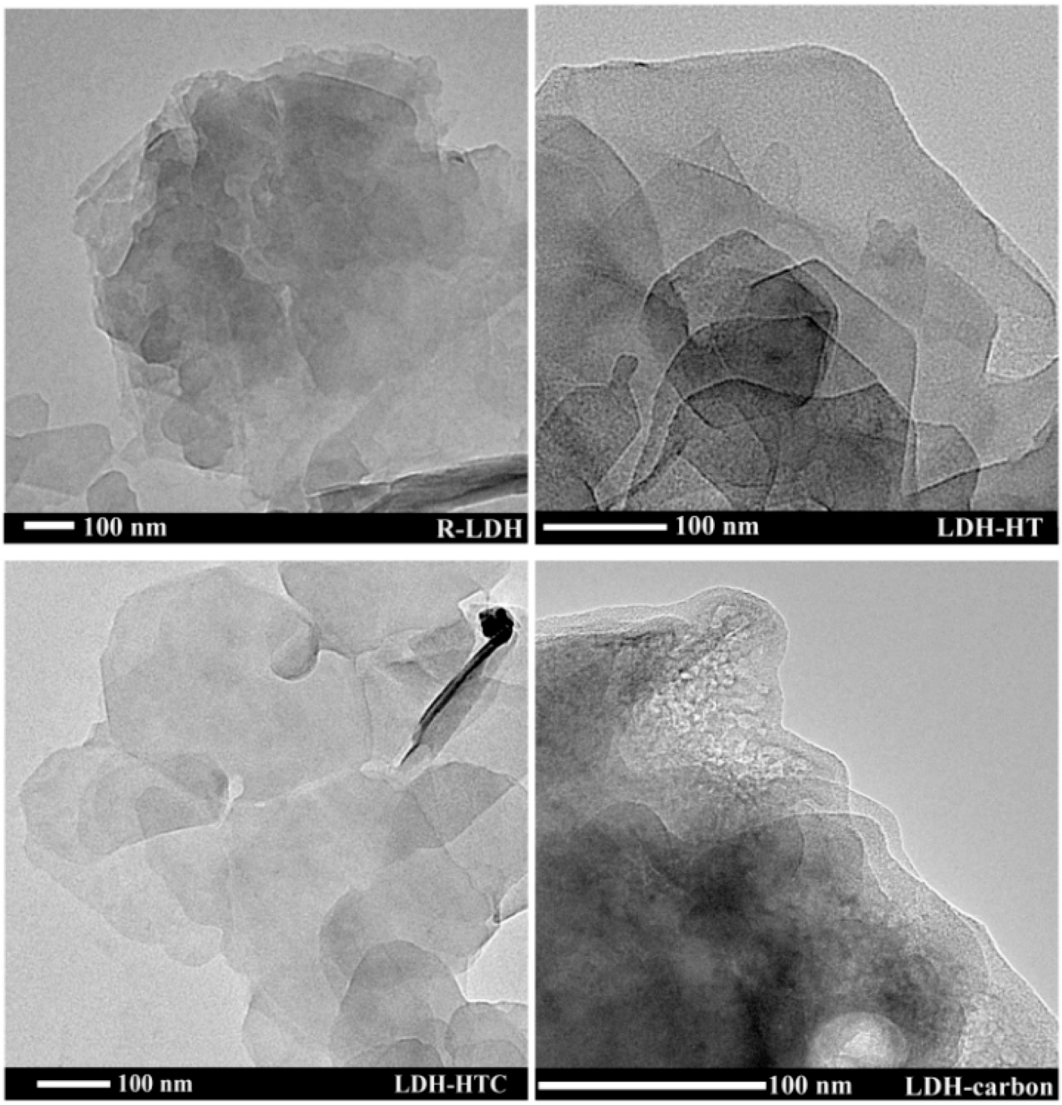

Fig. 2. TEM images of the samples; all of the materials present sheet-like morphology. R-LDH in the figure represents the reconstructed LDH from CLDH via reaction with water.

165.2 eV, respectively) (Terzyk, 2001) with a much higher amount than that of sulfonic group become the dominant S-involved functional groups as suggested by the S 2p spectra of LDH-carbon. Deconvolution of the N 1 s spectra mainly yields five peaks which can be identified as pyridinic−N (C−N−C/C═N, ~398.6 eV) (Tan et al., 2018), graphitic-N/nitroso (~400.4 eV) (Pels et al., 1995; Tan et al., 2018), oxide-N (402.6 eV) (Balamurugan et al., 2016; Tan et al., 2018), nitro (406.2 eV) (Pels et al., 1995), and nitrate group (−NO_3, 407.8 eV) (Liu et al., 2017). Two types of carbonization methods show little difference in the types of N-involved groups, but the conventional high-temperature carbonization procedure possesses strength in producing graphitic-N or nitroso. Above results demonstrate that both hydrothermal and conventional carbonization strategies are able to produce ample functional groups; most importantly, the types and relative contents of the functional groups can be regulated by these two different carbonization strategies.

BET specific surface areas of these LDH/carbon nanosheets were detected (Table 1). R-LDH presents large BET specific surface areas (SSA, 105.1 m^2/g), but the combination of LDH and HTC decreases the SSA with a smallest BET SSA of 32.4 m^2/g for LDH-HTC. These results suggest that LDH and HTC will block the pores of each other. These results further indicate the existence of HTC in the interlayers of LDH, because the formation of "LDH layer-carbon layer-LDH layer" structures will prevent N_2 from entering the interlayers of LDH. Therefore, hydrothermal carbonization method has its limit in producing LDH/carbon nanosheets composites with large surface area, but will produce materials with "LDH layer-carbon layer-LDH layer" alternating interval layered structures. It was suggested that a material with ordered interval layered structures of the different species would enhance various properties (e.g., mechanical, barrier, and flame-retardant properties) of the composites (Ding et al., 2017). On the other hand, via conventional high-temperature carbonization strategy, LDH/carbon nanosheets composites with higher SSA than LDH can be produced as indicated by the highest SSA of LDH-carbon of 153.6 m^2/g. The large SSA may be because the changes of relative distribution of LDH and carbon nanosheets during the reconstruction of LDH structures via washing. The changes of relative distribution of LDH and carbon nanosheets cause the formation of LDH aggregate and carbon nanosheets aggregate, which results in the decrease of the blocked pores and increase of the available pores. According to the previous review, LDH/carbon nanosheets composites prepared from high-temperature carbonization method in this work possess higher SSA than those of many other LDH/carbon nanosheets composites (Cao et al., 2016).

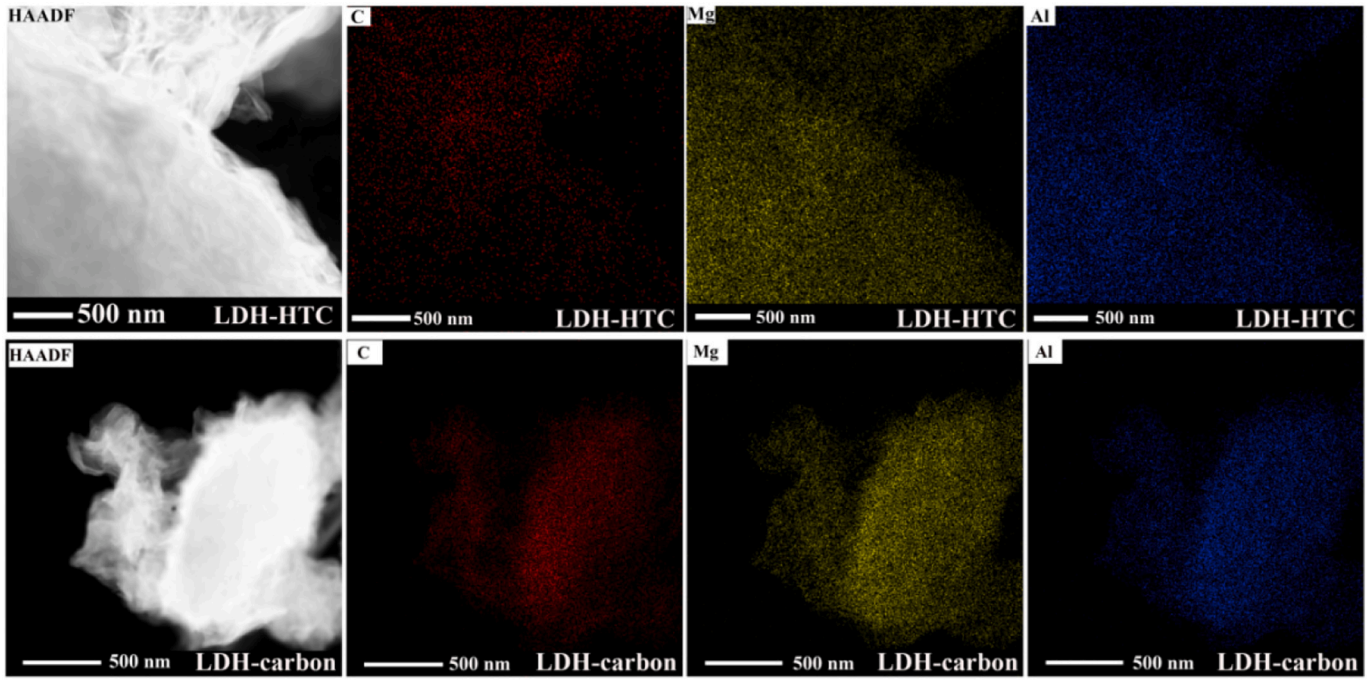

Fig. 3. STEM images of the LDH-HTC and LDH-carbon composites; carbon element is evenly distributed along with Mg and Al elements, indicating the uniform distribution of carbon nanosheets with LDH layers.

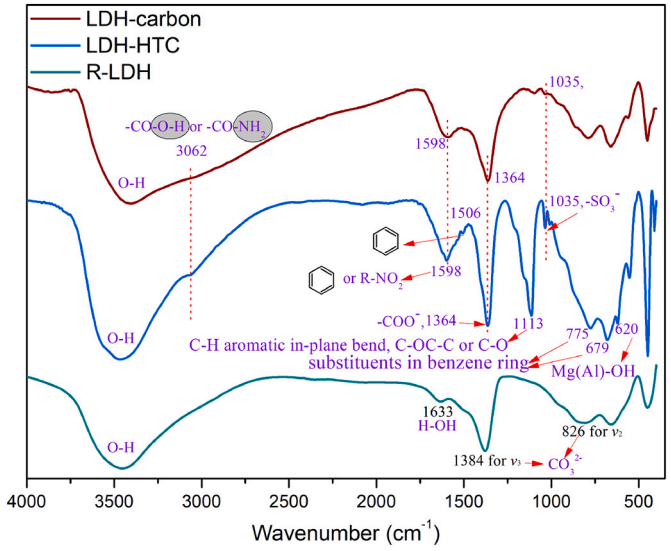

Fig. 4. FTIR spectra of R-LDH, LDH-HTC and LDH-carbon.

3.3. Adsorption performance of the composites

LDH/carbon composites such as LDH/graphene and LDH/graphene oxide are generally attractive and effective adsorbents for heavy metal ions, radionuclides, and organic contaminants due to their ample functional groups and/or large surface area (Cao et al., 2016; Daud et al., 2016; Huang et al., 2018; Linghu et al., 2017; Pang et al., 2019; Wang et al., 2020). Herein, we tested and compared the adsorption performance of the resultant LDH/carbon nanosheets composites toward heavy metal cation (Cd(II)) and anion (Cr(VI)). Fig. 6 shows the effect of contact time on Cr(VI) and Cd(II) adsorption capacity. The adsorption rates of Cr(VI) on the composites were very rapid and the adsorption reached completely equilibrium with 5 min, indicating strong interactions between Cr(VI) and the composites. Previous study also indicated that LDH could reach completely adsorption equilibrium of Cr(VI) within 8 min (Zhang et al., 2017). As for Cd(II) adsorption, the adsorption rates are much lower than those of Cr(VI) adsorption; c.a. 300 min is needed to reach adsorption equilibrium. Thus, to reach completely adsorption equilibrium, the contact time in the studies of effect of concentration set as 12 h. pH affects the adsorption performance significantly (Fig. 7). For Cr(VI) adsorption, the adsorption capacities on LDH/carbon composites decrease (from c.a. 35 to 20 mg/g; initial Cr(VI) concentration of 50 mg/L) with increasing pH from 3.0 to 10.0. For Cd(II) adsorption, opposite results were obtained, i.e., the adsorption capacities increase (from c.a. 12 to maximum of 35 mg/g; initial Cd(II) concentration of 50 mg/L) with increasing pH from 3.0 to 10.0. One obvious merit should be noted that the LDH-HTC and LDH-carbon composites both have strong pH buffer performance to resist the low pH and increase the pH from low value to c.a. 7.

The adsorption isotherms (Fig. 8) show that LDH-HTC, LDH-carbon, R-LDH, LDH-HT, and LDH-OII have Cr(VI) adsorption capacities of 28.9, 35.6, 8.0, 6.4, and 14.0 mg/g, respectively; Cd(II) adsorption capacities of 46.1, 48.5, 7.3, 8.5, and 15.1 mg/g, respectively. The composites (LDH-HTC and LDH-carbon) present much higher adsorption capacities than those of the counterparts (i.e. R-LDH, LDH-HT, and LDH-OII), indicating the formation of carbon nanosheets remarkably promote the adsorptive performance. Specifically, the LDH/carbon nanosheets composites possess higher adsorption capacities with 3.3 to 4.4-fold and 5.3 to 6.7-fold increase of the adsorbed capacities respectively for Cr(VI) and Cd(II), comparing to those of R-LDH. R-LDH showing low Cr(VI) adsorption capacity is because the interlayer anions are CO_3^{2-} (Fig. 4) which is most difficult to be exchanged (Goh et al., 2008; Prasanna et al., 2006). And the low Cd(II) adsorption capacity should be due to the fact that positively charged LDH produce electrostatic repulsion to cations (Fig. 9). As shown in Fig. 9, R-LDH shows high surface positive charge (c.a. 45 mV) under experimental solution pH condition; the high positively surface charge will prevent the adsorption of Cd(II) cation. Via calcination of MgAl-LDH to eliminate interlayer CO_3^{2-} and introduction of OII to induce functional groups of C—SO_3 and C—OH from OII, LDH—OII shows higher Cr(VI) and Cd(II) adsorption capacities than those of R-LDH and LDH-HT. According to Fig. 9, introduction of OII can greatly reduce surface charge with a

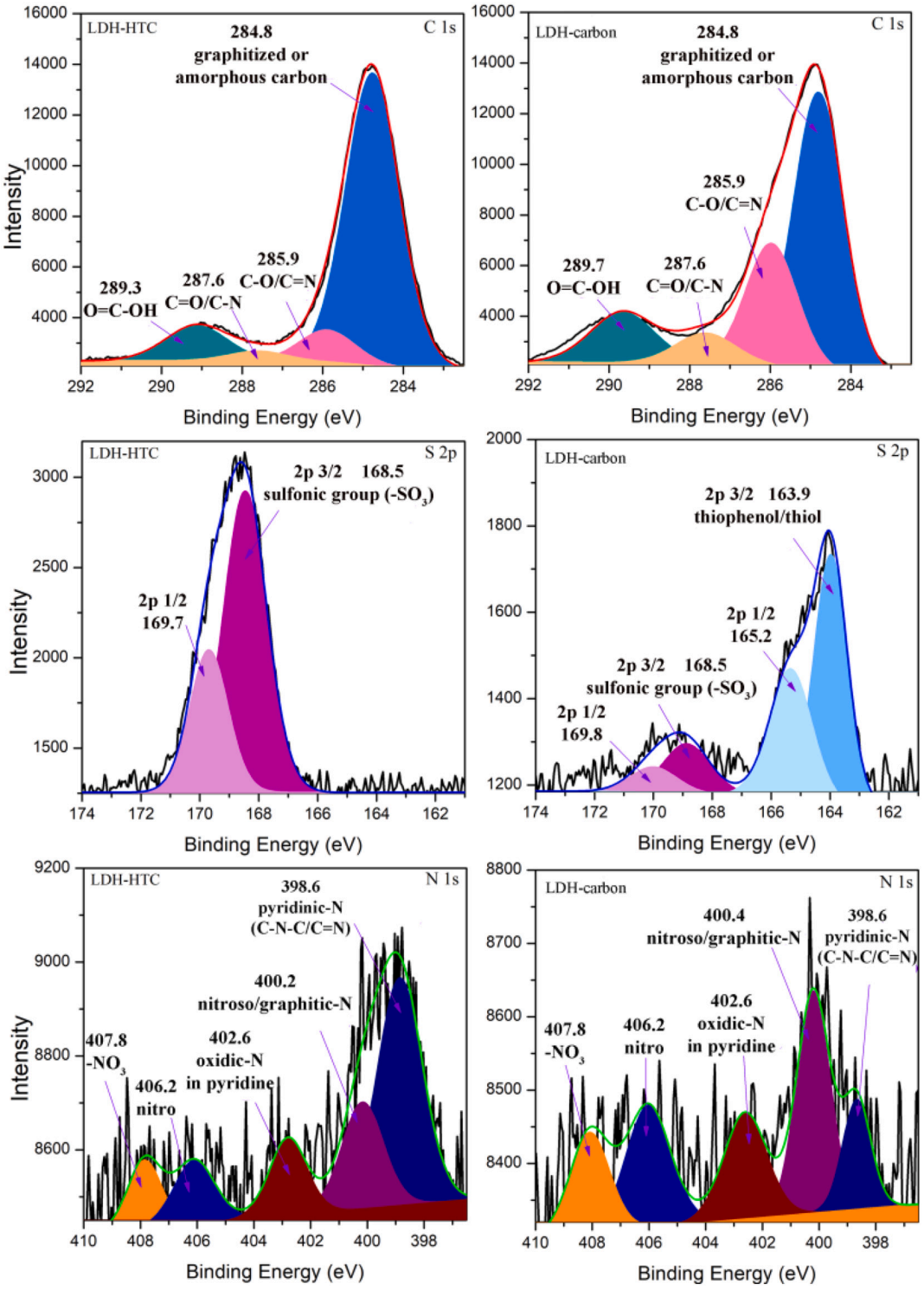

Fig. 5. C 1s, S 2p, and N 1s (from left to right) XPS spectra of LDH-HTC and LDH-carbon (from top to bottom); S and N elements come from the organic dyes OII.

Table 1
BET specific surface area of the materials. R-LDH in the table represents the reconstructed LDH from CLDH via reaction with water.

Sample	BET specific surface area (m^2/g)
R-LDH	105.1
LDH-HTC	32.4
LDH-carbon	153.6

value of c.a. 3.7 mV which is much lower than that of R-LDH at pH 7. The decrease of surface charge should therefore be one of the reasons for the increase of Cd(II) adsorption capacity. Other studies pointed out that when adsorbed enough anions on LDH, charge reversal would happen (Kentjono et al., 2010; Wei et al., 2011). For the LDH/carbon nanosheets composites, after carbonization, ample C, S, and N-involved functional groups are produced (Figs. 4 and 5). In addition, their surface charges are also much lower than those of R-LDH and LDH-HT. LDH-carbon and LDH-HTC show positively surface charge of 22.6 and

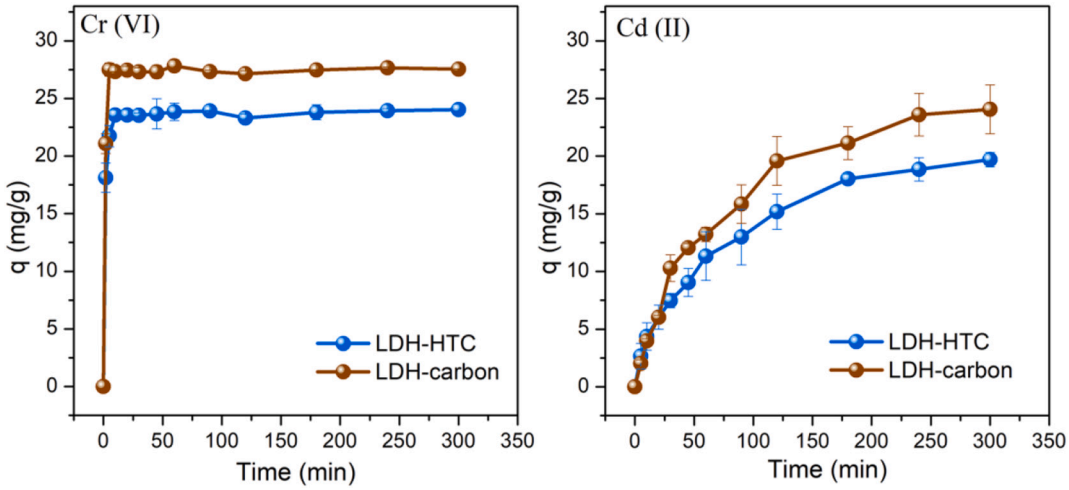

Fig. 6. Effect of contact time on the adsorption of Cr(VI) and Cd(II) (25 °C, pH 7.0, the dosage of the adsorbent is 1 g/L, and the initial concentrations of Cr(VI) and Cd (II) are both 50 mg/L).

4.5 mV at pH 7, respectively. These results may be the major reasons for the remarkable promotion of the adsorptive capacities of Cr(VI) and Cd (II) on these composites of LDH/carbon nanosheets. According to the XRD results of the samples after Cr(VI) adsorption (Fig. 10a), ion exchange is not the major mechanism for Cr(VI) removal; but for LDH-HTC, the adsorption of Cr(VI) caused the secondary arrangement of the interlayer anions indicated by the changes of d(003) values, suggesting the existence of electrostatic adsorption mechanism. FTIR spectra of the LDH/carbon composites before and after Cd(II) adsorption show no obvious changes with the maximum chemical shift of 2 cm^{-1} (Fig. 10b), indicating that no strong interaction between Cd(II) and surface functional groups of the adsorbents exists. These results suggest that the adsorption of Cd(II) is mainly via physical interaction. Huang et al. also got similar results when applying LDH/graphene oxide composite to remove Cd(II), Cu(II), and Pb(II); their results showed no obvious changes of the FTIR spectra before and after adsorption. (Huang et al., 2018).

Adsorption performance of the composites prepared from different carbonization strategies also presents differences. LDH-carbon has the higher adsorption capacities for both Cr(VI) and Cd(II) than those of LDH-HTC. It is suggested that functional groups and SSA are critical in improving activities of LDH/carbon composite (Cao et al., 2016; Daud et al., 2016). LDH-carbon has the highest adsorption capacities probably due to the fact that it has the largest SSA and highest amount of C-involved functional groups and thiophenol/thiol groups (see Table 1 and Fig. 5). However, the adsorption capacities for per surface area of LDH-HTC for both Cr(VI) (0.89 mg/m^2) and Cd(II) (1.42 mg/m^2) are much larger (c.a. 4-fold) than those of LDH-carbon (0.23 mg/m^2 for Cr (VI) and 0.32 mg/m^2 for Cd(II)). The different adsorption performance may be resulted from the differences in the types and amounts of S-involved functional groups, since sulfonic groups are the only S-involved functional groups for LDH-HTC with much higher amount than that of LDH-carbon, while thiophenol/thiol groups are the dominant groups for LDH-carbon.

Adsorption performance of the composites is also compared with those of reported LDH-based composites and other adsorbents. Huang et al. applied their magnetic MgAl-LDH/graphene oxide nano composites as Cd(II) adsorbents with maximum adsorbed amount of c.a. 20 mg/g at initial Cd(II) concentration of 80 mg/L (pH 7.0) (Huang et al., 2018). In the same conditions, Cd(II) adsorption capacities of the LDH/carbon nanosheets composites in this work reach higher values between 20 and 30 mg/g. The comparison of the removal performance of Cd(II) and Cr(VI) between the materials in this study and various other materials is shown in Table 2. As can be seen, the resultant LDH/carbon nanosheets composites in this study can be sufficient adsorbents for heavy metal ions.

3.4. Regeneration of the adsorbents

As displayed in Fig. 11, the adsorption capacities of Cr(VI) and Cd

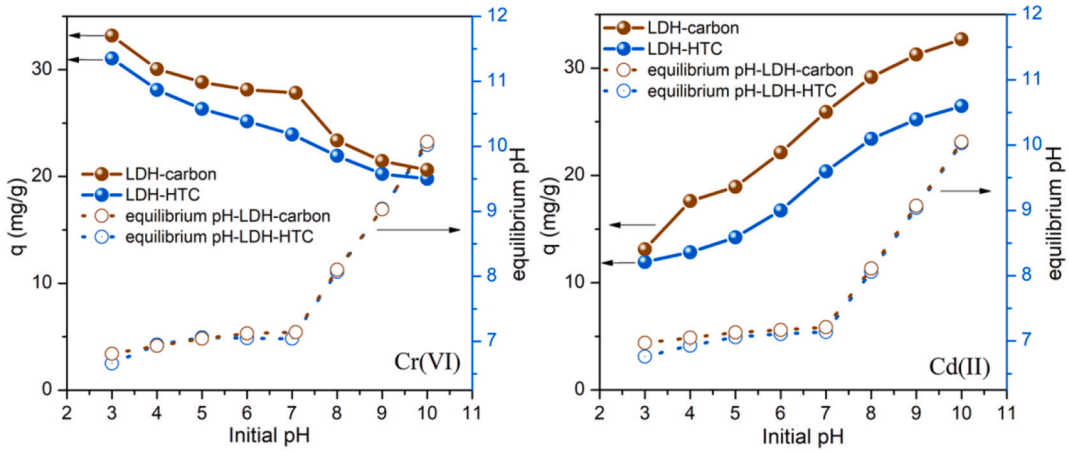

Fig. 7. Effect of pH on the adsorption of Cr(VI) and Cd(II) (25 °C, the dosage of the adsorbent is 1 g/L, and the initial concentrations of Cr(VI) and Cd(II) are both 50 mg/L).

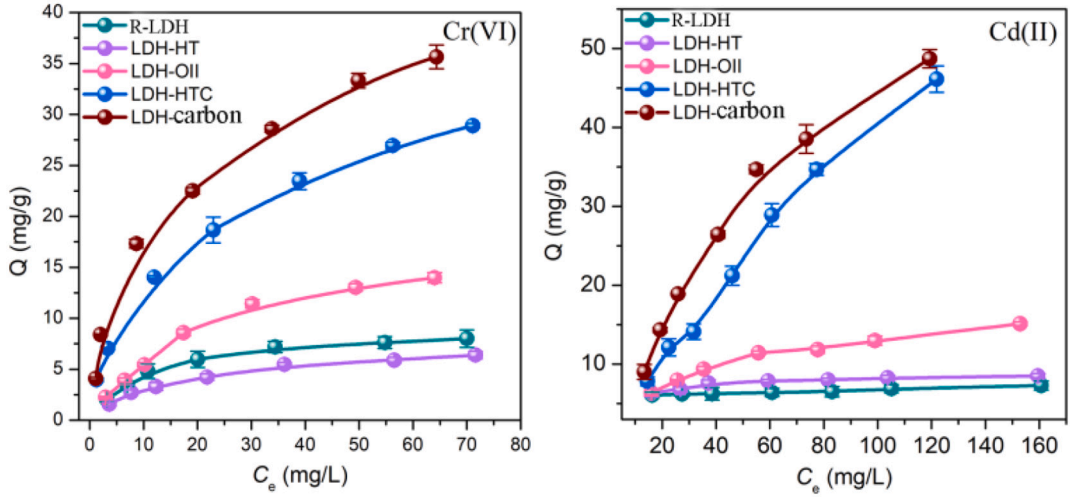

Fig. 8. Cr(VI) and Cd(II) adsorption isotherms (25 °C, pH 7.0, the dosage of the adsorbent is 1 g/L, and the initial concentration of Cr(VI) and Cd(II) is 5–100 mg/L and 22.4–168 mg/L, respectively, contact time is 12 h).

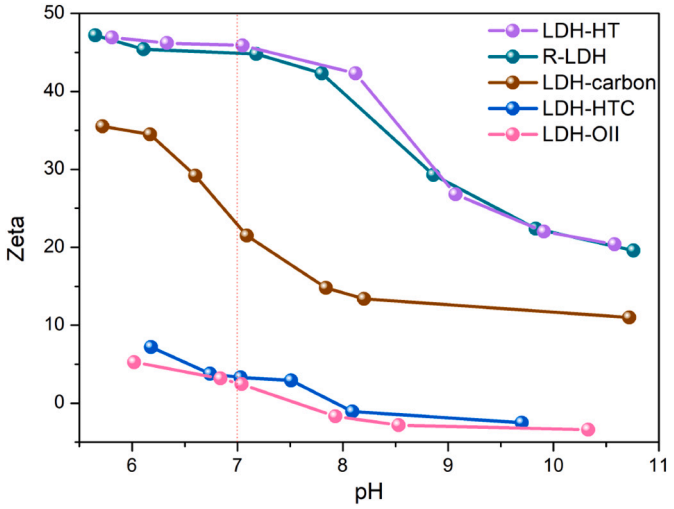

Fig. 9. Variation of zeta potential of the samples with pH.

(II) on the regenerated LDH-carbon and LDH-HTC first increase and then decrease. The improvement of Cr(VI) adsorption performance in cycle 1 may be ascribed to the introduction of easily exchangeable anions of Cl^- when regeneration of the adsorbents by using Cl^- (NaCl) to exchange Cr(VI). For the improvement of adsorption performance for Cd(II) in cycle 1, the reason may be the introduced CH_3COO^- on the adsorbents offering extra adsorption sites for Cd(II). According to the previous studies, COO^- showed good affinity to Cd(II) (Min et al., 2004). After 5 times of cycle, the adsorbents still retain 63.3–68.5% of their initial adsorption capacities (i.e., the values in cycle 0).

4. Conclusions

In conclusion, LDH/carbon nanosheets composites were facilely prepared by in-situ formation of carbon nanosheets via carbonization of organic LDH. Hydrothermal carbonization and high-temperature carbonization plus reaction with water were demonstrated to be effective methods to prepare composites of LDH/carbon nanosheets. The methods make it readily to prepare carbon nanosheets with varied C, S, and N-involved functional groups. Most importantly, the types and relative contents of the functional groups can be regulated by these two different carbonization strategies. As for C-involved functional groups, hydroxyl/C═N and carboxyl are the dominant functional groups for the LDH/carbon nanosheets, but different carbonization treatment can adjust their relative contents. Hydrothermal carbonization led to higher amount of carboxyl than that of hydroxyl/C═N groups, while conventional carbonization treatment caused a higher amount of hydroxyl/C═N than that of carboxyl. With regard to S-involved functional groups, sulfonic and thiophenol/thiol are the major functional groups. Hydrothermal carbonization retained sulfonic group from organic compounds (OII) and produced no other S-involved functional groups. However, via high-temperature carbonization treatment, thiophenol/thiol becomes the dominant functional groups with small amount of sulfonic group. On the other hand, these two different carbonization strategies can also cause large differences in specific surface area of the composites with the high-temperature carbonized product possessing a much larger value than that of hydrothermal sample.

The obtained materials can be used as effective multifunctional adsorbents for both anionic (Cr(VI)) and cationic (Cd(II)) contaminants. The carbon nanosheets can remarkably promote the adsorptive performance, with maximum adsorption capacities of 4.4-fold and 6.7-fold increase respectively for Cr(VI) and Cd(II), comparing to those of LDH. The elimination of interlaminar carbonates, decrease of surface positive charge, and the introduction of various functional groups produced by the formation of carbon nanosheets may be the major reasons for the enhanced adsorptive performance. For the two LDH/carbon nanosheets composites, LDH-carbon shows higher adsorption performance than LDH-HTC for both Cr(VI) and Cd(II), but the adsorption capacities for per surface area of LDH-HTC for both Cr(VI) (0.89 mg/m^2) and Cd(II) (1.42 mg/m^2) are much larger (c.a. 4-fold) than those of LDH-carbon (0.23 mg/m^2 for Cr(VI) and 0.32 mg/m^2 for Cd(II)). The different adsorption performance may be resulted from the differences in the types and amounts of S-involved functional groups. Apart from heavy metal removal, we believe LDH/carbon nanosheets may also be valuable materials for other fields such as energy and catalysis fields as suggested by various reported LDH/carbon nanosheets composites. This work provides facile ways for preparation of LDH/carbon nanosheets materials, which may also be ways for recycling of waste organic clay and organic clay minerals by producing functional materials.

Declaration of Competing Interest

The authors declare that they have no known competing financial interests or personal relationships that could have appeared to influence the work reported in this paper.

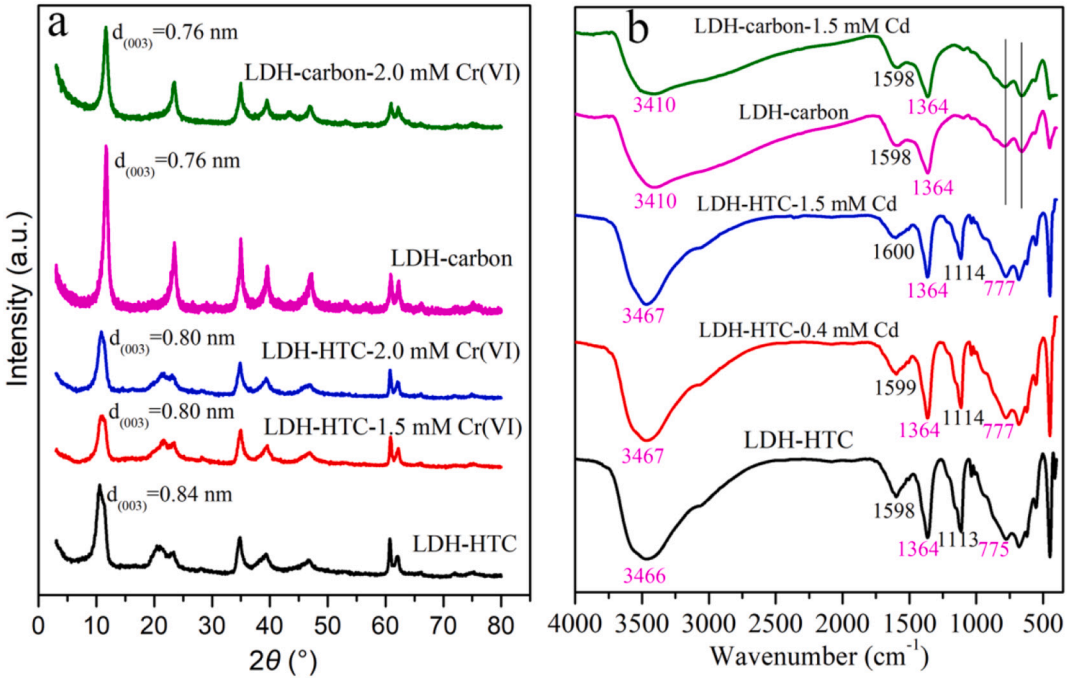

Fig. 10. XRD patterns of the samples after adsorption of Cr(VI) (a) and FTIR spectra of the samples after adsorption of Cd(II). "LDH-carbon-2.0 mM Cr(VI)" represents solid generated from adsorption of 2.0 mM Cr(VI) by using LDH-carbon as adsorbent; other samples share same nomenclature.

Table 2
Maximum adsorption capacities (Q_m) of Cd(II) and Cr(VI) on various materials.

Material	Pollutant	C_0 (mg/L)	pH	Q_m (mg/g)	Ref.
Inorganic and inorganic-organic montmorillonite	Cd(II)	30–210	5.0	23.1	(Ma et al., 2015, 2016)
MgAl-LDH/humate	Cd(II)	0–280	5.0–9.0	42.6	(González et al., 2015)
MgAl-LDH/chitosan	Cd(II)	0–100	7.0	39.7	(Lyu et al., 2019)
MgAl-LDH/magnetic graphene oxide	Cd(II)	5–300	6.0	45.1	(Huang et al., 2018)
LDH/carbon nanosheets	Cd(II)	22.4–168	7.0	48.5	this work
FeOOH/activated carbon	Cr(VI)	5–500	5.6	27.6	(Su et al., 2019)
Fe_3O_4/graphene oxide	Cr(VI)	0–50	4.5	32.3	(Liu et al., 2013)
MgAl-LDH	Cr(VI)	0–100	6.0	17.0	(Lazaridis et al., 2004)
NiFe-LDH/graphene oxide	Cr(VI)	0–90	6.0–7.0	47.0	(Zheng et al., 2019)
LDH/carbon nanosheets	Cr(VI)	5–100	7.0	35.6	This work

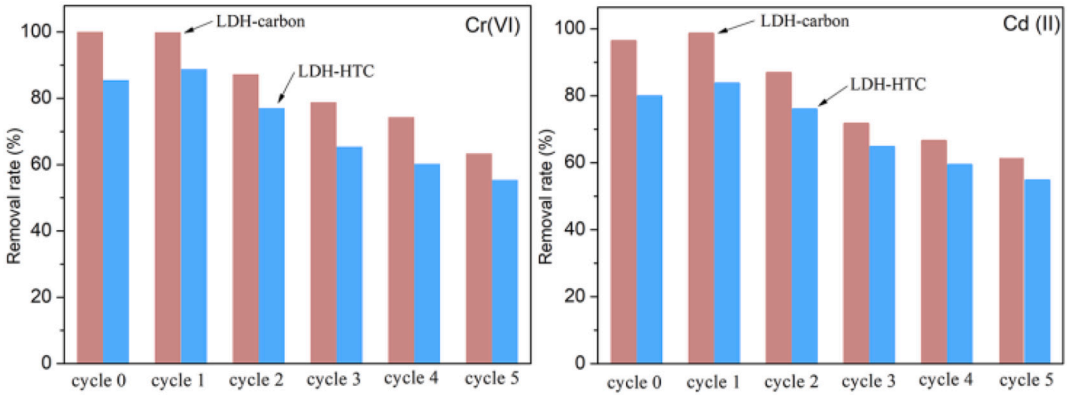

Fig. 11. Reusability test on the regenerated LDH-carbon and LDH-HTC. The dosage of the adsorbents is 2 g/L; initial concentrations of Cr(VI) and Cd(II) are 50 and 30 mg/L, respectively; adsorption pH and contact time are respectively 7.0 and 12 h.

Acknowledgements

M. L. acknowledges the financial support from the National Natural Science Foundation of China (41902039) and the China Postdoctoral Science Foundation (2018M640832); R. Z. thanks the financial support from the National Natural Science Foundation of China (41572031); Y. X. thanks the financial support from the National Natural Science Foundation of China (51678511). This is contribution No. IS-2914 from GIGCAS.

Appendix A. Supplementary data

Supplementary data to this article can be found online at https://doi.org/10.1016/j.clay.2020.105867.

References

Aregay, G.G., Jawad, A., Du, Y., Shahzad, A., Chen, Z., 2019. Efficient and selective removal of chromium (VI) by sulfide assembled hydrotalcite compounds through concurrent reduction and adsorption processes. J. Mol. Liq. 294, 111532.

Balamurugan, J., Thanh, T.D., Kim, N.H., Lee, J.H., 2016. Facile synthesis of 3D hierarchical N-doped graphene nanosheet/cobalt encapsulated carbon nanotubes for high energy density asymmetric supercapacitors. J. Mater. Chem. A 4, 9555–9565.

Cao, Y., Li, G., Li, X., 2016. Graphene/layered double hydroxide nanocomposite: properties, synthesis, and applications. Chem. Eng. J. 292, 207–223.

Chen, Q., Zhu, R., Deng, W., Xu, Y., Zhu, J., Tao, Q., He, H., 2014. From used montmorillonite to carbon monolayer-montmorillonite nanocomposites. Appl. Clay Sci. 100, 112–117.

Chen, Q., Zhu, R., He, Q., Liu, S., Wu, D., Fu, H., Du, J., Zhu, J., He, H., 2019. In situ synthesis of a silicon flake/nitrogen-doped graphene-like carbon composite from organoclay for high-performance lithium-ion battery anodes. Chem. Commun. 55, 2644–2647.

Chen, W., Qu, B., 2003. Structural characteristics and thermal properties of PE-g-MA/MgAl-LDH exfoliation nanocomposites synthesized by solution intercalation. Chem. Mater. 15, 3208–3213.

Clearfield, A., Costantino, U., 1996. Layered metal phosphates and their intercalation chemistry. In: Alberti, G., Bein, T. (Eds.), Comprehensive Supramolecular Chemistry. Elsevier, Oxford, UK, pp. 107–149.

Colthup, N., 2012. Introduction to Infrared and Raman Spectroscopy. Elsevier.

Damodar, D., Kumar, S.K., Martha, S.K., Deshpande, A.S., 2018. Nitrogen-doped graphene-like carbon nanosheets from commercial glue: morphology, phase evolution and Li-ion battery performance. Dalton Trans. 47, 12218–12227.

Daud, M., Kamal, M.S., Shehzad, F., Al-Harthi, M.A., 2016. Graphene/layered double hydroxides nanocomposites: a review of recent progress in synthesis and applications. Carbon 104, 241–252.

Ding, F., Liu, J., Zeng, S., Xia, Y., Wells, K.M., Nieh, M.-P., Sun, L., 2017. Biomimetic nanocoatings with exceptional mechanical, barrier, and flame-retardant properties from large-scale one-step coassembly. Sci. Adv. 3, e1701212.

Goh, K.-H., Lim, T.-T., Dong, Z., 2008. Application of layered double hydroxides for removal of oxyanions: a review. Water Res. 42, 1343–1368.

González, M., Pavlovic, I., Barriga, C., 2015. Cu (II), Pb (II) and Cd (II) sorption on different layered double hydroxides. A kinetic and thermodynamic study and competing factors. Chem. Eng. J. 269, 221–228.

Gunjakar, J.L., Kim, I.Y., Lee, J.M., Lee, N.-S., Hwang, S.-J., 2013. Self-assembly of layered double hydroxide 2D nanoplates with graphene nanosheets: an effective way to improve the photocatalytic activity of 2D nanostructured materials for visible light-induced O 2 generation. Energy Environ. Sci. 6, 1008–1017.

Hou, H., Shao, L., Zhang, Y., Zou, G., Chen, J., Ji, X., 2017. Large-area carbon nanosheets doped with phosphorus: a high-performance anode material for sodium-ion batteries. Adv. Sci. 4.

Huang, Q., Chen, Y., Yu, H., Yan, L., Zhang, J., Wang, B., Du, B., Xing, L., 2018. Magnetic graphene oxide/MgAl-layered double hydroxide nanocomposite: one-pot solvothermal synthesis, adsorption performance and mechanisms for Pb2+, Cd2+, and Cu2+. Chem. Eng. J. 341, 1–9.

Jain, A., Balasubramanian, R., Srinivasan, M., 2016. Hydrothermal conversion of biomass waste to activated carbon with high porosity: a review. Chem. Eng. J. 283, 789–805.

Jawad, A., Liao, Z., Zhou, Z., Khan, A., Wang, T., Ifthikar, J., Shahzad, A., Chen, Z., Chen, Z., 2017. Fe-MoS4: an effective and stable LDH-based adsorbent for selective removal of heavy metals. ACS Appl. Mater. Interfaces 9, 28451–28463.

Jawad, A., Peng, L., Liao, Z., Zhou, Z., Shahzad, A., Ifthikar, J., Zhao, M., Chen, Z., Chen, Z., 2019. Selective removal of heavy metals by hydrotalcites as adsorbents in diverse wastewater: different intercalated anions with different mechanisms. J. Clean. Prod. 211, 1112–1126.

Jawad, A., Wang, H., Ifthikar, J., Khan, A., Wang, T., Zhan, K., Shahzad, A., Chen, Z., Chen, Z., 2018. Efficient, stable and selective adsorption of heavy metals by thio-functionalized layered double hydroxide in diverse types of water. Chem. Eng. J. 332, 387–397.

Kentjono, L., Liu, J., Chang, W., Irawan, C., 2010. Removal of boron and iodine from optoelectronic wastewater using Mg–Al (NO 3) layered double hydroxide. Desalination 262, 280–283.

Khan, A., Nurnabi, M., Bala, P., 2009. Studies on thermal transformation of Na–montmorillonite–glycine intercalation compounds. JTAC 96, 929–935.

Koilraj, P., Kamura, Y., Sasaki, K., 2018a. Cosorption characteristics of SeO42- and Sr2+ radioactive surrogates using 2D/2D graphene oxide-layered double hydroxide nanocomposites. ACS Sustain. Chem. Eng. 6, 13854–13866.

Koilraj, P., Kamura, Y., Sasaki, K., 2018b. Synergetic co-immobilization of SeO42- and Sr2+ from aqueous solution onto multifunctional graphene oxide and carbon-dot based layered double hydroxide nanocomposites and their mechanistic investigation. J. Mater. Chem. A 6, 10008–10018.

Laipan, M., Fu, H., Zhu, R., Rivera, L., Zhu, G., Zhu, J., He, H., 2017a. Photochemically induced electron transfer: simultaneously decolorizing dye and reducing Cr (VI). Water Air Soil Pollut. 228, 446.

Laipan, M., Fu, H., Zhu, R., Sun, L., Steel, R.M., Ye, S., Zhu, J., He, H., 2018. Calcined Mg/Al-LDH for acidic wastewater treatment: simultaneous neutralization and contaminant removal. Appl. Clay Sci. 153, 46–53.

Laipan, M., Fu, H., Zhu, R., Sun, L., Zhu, J., He, H., 2017b. Converting spent Cu/Fe layered double hydroxide into Cr(VI) reductant and porous carbon material. Sci. Rep. 7.

Laipan, M., Xiang, L., Yu, J., Martin, B.R., Zhu, R., Zhu, J., He, H., Clearfield, A., Sun, L., 2020a. Layered intercalation compounds: mechanisms, new methodologies, and advanced applications. PrMS 109.

Laipan, M., Zhu, R., Chen, Q., Zhu, J., Xi, Y., Ayoko, G.A., He, H., 2015. From spent Mg/Al layered double hydroxide to porous carbon materials. J. Hazard. Mater. 300, 572–580.

Laipan, M., Zhu, R., Zhu, J., He, H., 2016. Visible light assisted Fenton-like degradation of Orange II on Ni 3 Fe/Fe 3 O 4 magnetic catalyst prepared from spent FeNi layered double hydroxide. J. Mol. Catal. A Chem. 415, 9–16.

Laipan, M.W., Yu, J.F., Zhu, R.L., Zhu, J.X., Smith, A.T., He, H.P., O'Hare, D., Sun, L.Y., 2020b. Functionalized layered double hydroxides for innovative applications. Mater. Horiz. 7, 715–745.

Larkin, P., 2017. Infrared and Raman Spectroscopy: Principles and Spectral Interpretation. Elsevier.

Latham, K.G., Dose, W.M., Allen, J.A., Donne, S.W., 2018. Nitrogen doped heat treated and activated hydrothermal carbon: NEXAFS examination of the carbon surface at different temperatures. Carbon 128, 179–190.

Lazaridis, N.K., Pandi, T.A., Matis, K.A., 2004. Chromium(VI) removal from aqueous solutions by Mg-Al-CO3 hydrotalcite: sorption-desorption kinetic and equilibrium studies. Ind. Eng. Chem. Res. 43, 2209–2215.

Le, K., Wang, Z., Wang, F., Wang, Q., Shao, Q., Murugadoss, V., Wu, S., Liu, W., Liu, J., Gao, Q., Guo, Z., 2019. Sandwich-like NiCo layered double hydroxide/reduced graphene oxide nanocomposite cathodes for high energy density asymmetric supercapacitors. Dalton Trans. 48, 5193–5202.

Li, C., Wei, M., Evans, D.G., Duan, X., 2014. Layered double hydroxide-based nanomaterials as highly efficient catalysts and adsorbents. Small 10, 4469–4486.

Li, H., Zhu, G., Liu, Z.-H., Yang, Z., Wang, Z., 2010. Fabrication of a hybrid graphene/layered double hydroxide material. Carbon 48, 4391–4396.

Linghu, W., Yang, H., Sun, Y., Sheng, G., Huang, Y., 2017. One-pot synthesis of LDH/GO composites as highly effective adsorbents for decontamination of U (VI). ACS Sustain. Chem. Eng. 5, 5608–5616.

Liu, J., Zhu, R., Chen, Q., Zhou, H., Liang, X., Ma, L., Parker, S.C., 2019. The significant effect of photo-catalyzed redox reactions on the immobilization of chromium by hematite. Chem. Geol. 524, 228–236.

Liu, M., Wen, T., Wu, X., Chen, C., Hu, J., Li, J., Wang, X., 2013. Synthesis of porous Fe3O4 hollow microspheres/graphene oxide composite for Cr(VI) removal. Dalton Trans. 42, 14710–14717.

Liu, X., Liu, J., Zheng, B., Yan, L., Dai, J., Zhuang, Z., Du, J., Guo, Y., Xiao, D., 2017. N-doped carbon dots: green and efficient synthesis on a large-scale and their application in fluorescent pH sensing. New J. Chem. 41, 10607–10612.

Lyu, F., Yu, H., Hou, T., Yan, L., Zhang, X., Du, B., 2019. Efficient and fast removal of Pb2+ and Cd2+ from an aqueous solution using a chitosan/Mg-Al-layered double hydroxide nanocomposite. J. Colloid Interface Sci. 539, 184–193.

Ma, L., Wang, Q., Islam, S.M., Liu, Y., Ma, S., Kanatzidis, M.G., 2016. Highly selective and efficient removal of heavy metals by layered double hydroxide intercalated with the MoS42-ion. J. Am. Chem. Soc. 138, 2858–2866.

Ma, S., Huang, L., Ma, L., Shim, Y., Islam, S.M., Wang, P., Zhao, L.-D., Wang, S., Sun, G., Yang, X., 2015. Efficient uranium capture by polysulfide/layered double hydroxide composites. J. Am. Chem. Soc. 137, 3670–3677.

Mallakpour, S., Behranvand, V., 2017. Water sanitization by the elimination of Cd2+ using recycled PET/MWNT/LDH composite: morphology, thermal, kinetic, and isotherm studies. ACS Sustain. Chem. Eng. 5, 5746–5757.

Min, S.H., Han, J.S., Shin, E.W., Park, J.K., 2004. Improvement of cadmium ion removal by base treatment of juniper fiber. Water Res. 38, 1289–1295.

Miyata, S., 1980. Physico-chemical properties of synthetic hydrotalcites in relation to composition. Clay Clay Miner. 28, 50–56.

Nizamuddin, S., Baloch, H.A., Griffin, G., Mubarak, N., Bhutto, A.W., Abro, R., Mazari, S.A., Ali, B.S., 2017. An overview of effect of process parameters on hydrothermal carbonization of biomass. Renew. Sust. Energ. Rev. 73, 1289–1299.

Pang, H., Wu, Y., Wang, X., Hu, B., Wang, X., 2019. Recent advances in composites of graphene and layered double hydroxides for water remediation: a review. Chem.-Asian J. 14, 2542–2552.

Pels, J.R., Kapteijn, F., Moulijn, J.A., Zhu, Q., Thomas, K.M., 1995. Evolution of nitrogen functionalities in carbonaceous materials during pyrolysis. Carbon 33, 1641–1653.

Peng, H.H., Chen, J., Jiang, D.Y., Guo, X.L., Chen, H., Zhang, Y.X., 2016. Merging of memory effect and anion intercalation: MnOx-decorated MgAl-LDO as a high-performance nano-adsorbent for the removal of methyl orange. Dalton Trans. 45, 10530–10538.

Prasanna, S.V., Rao, R.A.P., Kamath, P.V., 2006. Layered double hydroxides as potential chromate scavengers. JCIS 304, 292–299.

Rafiee, J., Mi, X., Gullapalli, H., Thomas, A.V., Yavari, F., Shi, Y., Ajayan, P.M., Koratkar, N.A., 2012. Wetting transparency of graphene. Nat. Mater. 11, 217.

Su, M., Fang, Y., Li, B., Yin, W., Gu, J., Liang, H., Li, P., Wu, J., 2019. Enhanced hexavalent chromium removal by activated carbon modified with micro-sized goethite using a facile impregnation method. Sci. Total Environ. 647, 47–56.

Sun, J., Liu, H., Chen, X., Evans, D.G., Yang, W., Duan, X., 2012. Synthesis of graphene nanosheets with good control over the number of layers within the two-dimensional galleries of layered double hydroxides. Chem. Commun. 48, 8126–8128.

Tan, A.-D., Wan, K., Wang, Y.-F., Fu, Z.-Y., Liang, Z.-X., 2018. N, S-containing MOF-derived dual-doped mesoporous carbon as a highly effective oxygen reduction reaction electrocatalyst. Catal. Sci. Technol. 8, 335–343.

Terzyk, A.P., 2001. The influence of activated carbon surface chemical composition on

the adsorption of acetaminophen (paracetamol) in vitro: Part II. TG, FTIR, and XPS analysis of carbons and the temperature dependence of adsorption kinetics at the neutral pH. Colloids Surf. A Physicochem. Eng. Asp. 177, 23–45.
Wan, J., Lacey, S.D., Dai, J., Bao, W., Fuhrer, M.S., Hu, L., 2016. Tuning two-dimensional nanomaterials by intercalation: materials, properties and applications. ChSRv 45, 6742–6765.
Wang, H., Wang, S., Chen, Z., Zhou, X., Wang, J., Chen, Z., 2020. Engineered biochar with anisotropic layered double hydroxide nanosheets to simultaneously and efficiently capture Pb2+ and CrO42-from electroplating wastewater. Bioresour. Technol. 306, 123118.
Wang, Q., O'Hare, D., 2012. Recent advances in the synthesis and application of layered double hydroxide (LDH) nanosheets. Chem. Rev. 112, 4124–4155.
Wei, Y.-P., Wei, D.-Q., Gao, H.-W., 2011. Treatment of dye wastewater by in situ hybridization with Mg–Al layered double hydroxides and reuse of dye sludge. Chem. Eng. J. 172, 872–878.
Wen, G., Wang, B., Wang, C., Wang, J., Tian, Z., Schlögl, R., Su, D.S., 2017. Hydrothermal carbon enriched with oxygenated groups from biomass glucose as an efficient carbocatalyst. Angew. Chem. Int. Ed. 56, 600–604.
Whittingham, M.S., Jacobson, A.J. (Eds.), 1982. Intercalation Chemistry. Academic Press.
Xu, Y., Huang, W., Chen, X., Ge, F., Zhu, R., Sun, L., 2018. Self-assembled ZnAl-LDH/PMo12 nano-hybrids as effective catalysts on the degradation of methyl orange under room temperature and ambient pressure. Appl. Catal. A Gen. 550 (8).
Yang, D., Velamakanni, A., Bozoklu, G., Park, S., Stoller, M., Piner, R.D., Stankovich, S., Jung, I., Field, D.A., Ventrice Jr., C.A., 2009. Chemical analysis of graphene oxide films after heat and chemical treatments by X-ray photoelectron and Micro-Raman spectroscopy. Carbon 47, 145–152.
Yao, Q.-S., Li, Z.-C., Qiu, Z.-M., Zhang, F., Chen, X.-B., Chen, D.-C., Guan, S.-K., Zeng, R.-C., 2019. Corrosion resistance of Mg (OH) 2/Mg–Al-layered double hydroxide coatings on magnesium alloy AZ31: influence of hydrolysis degree of silane. Rare Metals 38, 629–641.
Yu, J., Martin, B.R., Clearfield, A., Luo, Z., Sun, L., 2015. One-step direct synthesis of layered double hydroxide single-layer nanosheets. Nanoscale 7, 9448–9451.
Yu, J., Wang, Q., O'Hare, D., Sun, L., 2017a. Preparation of two dimensional layered double hydroxide nanosheets and their applications. Chem. Soc. Rev. 46, 5950–5974.
Yu, S., Wang, J., Song, S., Sun, K., Li, J., Wang, X., Chen, Z., Wang, X., 2017b. One-pot synthesis of graphene oxide and Ni-Al layered double hydroxides nanocomposites for the efficient removal of U (VI) from wastewater. SCIENCE CHINA Chem. 60, 415–422.
Zhang, B., Luan, L., Gao, R., Li, F., Li, Y., Wu, T., 2017. Rapid and effective removal of Cr (VI) from aqueous solution using exfoliated LDH nanosheets. Colloids Surf. A Physicochem. Eng. Asp. 520, 399–408.
Zhao, X., Cao, J.-P., Zhao, J., Hu, G.-H., Dang, Z.-M., 2014. A hybrid Mg-Al layered double hydroxide/graphene nanostructure obtained via hydrothermal synthesis. Chem. Phys. Lett. 605, 77–80.
Zhao, Y., Li, J.-G., Fang, F., Chu, N., Ma, H., Yang, X., 2012. Structure and luminescence behaviour of as-synthesized, calcined, and restored MgAlEu-LDH with high crystallinity. Dalton Trans. 41, 12175–12184.
Zheng, Y., Cheng, B., You, W., Yu, J., Ho, W., 2019. 3D hierarchical graphene oxide-NiFe LDH composite with enhanced adsorption affinity to Congo red, methyl orange and Cr(VI) ions. J. Hazard. Mater. 369, 214–225.
Zhou, J.-H., Sui, Z.-J., Zhu, J., Li, P., Chen, D., Dai, Y.-C., Yuan, W.-K., 2007. Characterization of surface oxygen complexes on carbon nanofibers by TPD, XPS and FT-IR. Carbon 45, 785–796.